Explicit dynamics "SPH – Finite Element" coupling using the Arlequin method

Simulation of projectile's impacts on concrete slabs

Yann Chuzel-Marmot* — Alain Combescure* — Roland Ortiz**

** LAboratoire de Mécanique des COntacts et des Structures*
INSA de Lyon
UMR/CNRS 5259, Bât. Jean d'Alembert
18-20 rue des sciences, F-69621Villeurbanne cedex
{Yann.Chuzel-Marmot, Alain.Combescure}@insa-lyon.fr

*** Office National d'Etudes et de Recherches Aérospatiales*
Centre de Lille
5 boulevard Paul Painlevé, F-59000 Lille cedex
Roland.Ortiz@onera.fr

ABSTRACT. *The Arlequin method gives a simple and effective framework to glue models using various formulations. It is extended here in explicit dynamics and used in order to link a zone showing ruptures by fragmentation meshed with Smoothed Particles Hydrodynamics (SPH) and a larger second undamaged one meshed with finite elements (FEM). This paper gives some details on the method implemented in the EUROPLEXUS code, its validation on simple benchmarks and a confrontation between numerical simulations and results of an experimental study of concrete slab resistance to projectile impacts.*

RÉSUMÉ. *La méthode Arlequin présente un cadre simple et efficace afin de coupler des modèles de formulations diverses. La méthode est étendue ici en dynamique explicite afin de coupler une zone présentant des ruptures par fragmentation, maillée avec la méthode particulaire Smoothed Particles Hydrodynamics (SPH), et une seconde zone, plus grande et non endommagée, maillée avec des éléments finis (FEM). Ce document détaille la méthode implémentée dans le code de calcul EUROPLEXUS, sa validation sur des cas tests simples et une comparaison entre les simulations et les résultats d'une étude expérimentale sur la résistance de dalles béton à l'impact de projectiles.*

KEYWORDS: *Arlequin method, coupling, meshless, Sph, explicit dynamics, projectile impact, concrete, Mazars.*

MOTS-CLÉS : *méthode Arlequin, couplage, meshless, Sph, dynamique explicite, impact, projectile, béton, Mazars.*

DOI:10.3166/REMN.17.737-748

REMN – 17/2008. Giens 2007, pages 737 to 748

1. Introduction

The SPH or Element Free Galerkin (EFG) methods are very efficient to simulate perforations with fragmentation. But, in the most industrial applications, the computation effort is CPU time consuming. Moreover, the perforations and fragmentations are usually limited to a geometrically confined zone: it is then tempting to use SPH method only for the perforated region and finite element in the rest of the domain. This observation naturally leads to couple a usual FEM model in the non-fragmented zone and a SPH method in the zone which could be damaged and fragmented.

This geometrical partition of space introduces the concept of subdomains, already developed in dynamics, *eg* in the FETI method by (Fahrat *et al.,* 1995), and its extension by (Gravouil *et al.,* 2001). The method used in these approaches is not directly transposable to the "SPH - FEM" coupling because of the difficulty to impose constrains on the boundary's SPH domain: SPH being based on the strong form of equilibrium equations, the imposition of mixed boundary conditions is not easy.

A complete overview of the methods, currently used for coupling meshed and meshless formulations, is described in the publication of Rabczuk, Xiao and Sauer (Rabczuk *et al.,* 2006). The coupling methods can be classified in four families according to the way the artificial coupling forces are introduced (the Master-Slave methods, "compatibility coupling", gluing with overlapping zone and hybrid approximation).

This article proposes a volume gluing method with an overlapping zone and it relies on the Arlequin method. One zone is discretised with FEM and the other with SPH particles. The formulation is based on the work of (Ben Dhia, 1998; Rateau, 2003) and is limited to an overlapping zone which is linear elastic but which may undergo large displacements.

2. Continuous problem presentation with coupling formulation

This paragraph details the method used for a problem governed by only one physic, defined on only one domain Ω but discretized with two different formulations, overlapping themselves partially. Thus, the initial undeformed domain is denoted Ω^0 and the deformed domain Ω. The domain Ω^0 is divided into two subdomains $\Omega^0{}_1$ and $\Omega^0{}_2$ overlapped on a volume $\Omega^0{}_g$. Hence, $\Omega^0{}_{1g}$ and $\Omega^0{}_{2g}$ are the part of each subdomain defined by:

$$\Omega_{1g}^0 = \Omega_1^0 \cap \Omega_g^0 \quad \textit{and} \quad \Omega_{2g}^0 = \Omega_2^0 \cap \Omega_g^0 \qquad [1]$$

The mechanical states must be identical in the volumes $\Omega^0{}_{1g}$ and $\Omega^0{}_{2g}$. The restriction of displacements in the overlapping volume is imposed to be identical.

The coupling operator is based on the strain and the kinetic energies partition between the overlapping subdomains $\Omega^0{}_{1g}$ and $\Omega^0{}_{2g}$.

These energies are balanced in each point $\underline{M}$ by weight parameter functions $\underline{\alpha(M)}$, $\underline{\beta(M)}$ which are a partition of unity in order to take into account only once the energies in the overlapping zone (the domain $\Omega^0{}_g$ is described twice: $\Omega^0{}_{1g}$ and $\Omega^0{}_{2g}$). The following distribution is chosen:

$$\begin{cases} W_g^{def} = \int\limits_{\Omega_g^0} \left[\alpha(\underline{M}) e_1^{def}(\underline{M}) + (1-\alpha(\underline{M})) e_2^{def}(\underline{M})\right] dV(\underline{M}) \\ W_g^{kin} = \int\limits_{\Omega_g^0} \left[\beta(\underline{M}) e_1^{kin}(\underline{M}) + (1-\beta(\underline{M})) e_2^{kin}(\underline{M})\right] dV(\underline{M}) \end{cases} \quad [2]$$

In this formula, $e^{def}{}_i$ (resp. $e^{kin}{}_i$) represent the density of strain (resp. kinetic) energy of the subdomain *i*. In the Arlequin formulation, each subdomain $\Omega^0{}_i$ independently respects the basic equations of continuum mechanic but is constrained by artificial coupling forces $\underline{C}_i$ (representing the influence of the other subdomain on this one) on the overlapping zone. The conservation of linear momentum in subdomain *i* is then:

$$\begin{aligned} &\frac{d}{dt}\left[\int\limits_{\Omega_i^0-\Omega_{ig}^0} \rho^0 \underline{v}_i \cdot dV^0 + \int\limits_{\Omega_{ig}^0} \beta_i \rho^0 \underline{v}_i \cdot dV^0\right] = \int\limits_{\Omega_i^0-\Omega_{ig}^0} \nabla_X \underline{\underline{P}}_i \cdot dV^0 \\ &+ \int\limits_{\Omega_{ig}} \alpha_i \nabla_X \underline{\underline{P}}_i \cdot dV^0 + \int\limits_{\Omega_i^0-\Omega_{ig}^0} \rho^0 \underline{f}_i \cdot dV^0 + \int\limits_{\Omega_{ig}} \beta_i \rho^0 \underline{f}_i \cdot dV^0 + \underline{C}_i \end{aligned} \quad [3]$$

with *i, index of the subdomain (i=1 or 2),*
ρ^0*, initial density,*
v*, velocity vector,*
P, transposed of the first Piola-Kirchhoff stress tensor,
F, body forces.

3. "SPH – FEM" coupling formulation

3.1. *How to model the coupling operator?*

The coupling operator is based on the Lagrange multipliers associated to the displacement vector. The coupling energy is then defined by the following scalar product:

$$W^{interface} = \int_{\Omega_g^0}^{T} \underline{\lambda} \cdot \left(\underline{u}^{SPH} - \underline{u}^{FE} \right) dV^0 \qquad [4]$$

with $\underline{\lambda}$, *the Lagrange multipliers,*
$\underline{u}$, *the displacement vector.*

3.2. *Choice of the weight parameter functions*

In the case of coupling with a SPH formulation, the choice of the weight parameter functions $(\underline{\alpha},\underline{\beta})$ is reduced: the SPH weighting functions do not allow high variations of the mechanical properties in the material. Hence, we choose linear weight parameter functions in the thickness of the overlapping zone, such as:

$$\left.\begin{array}{l} \alpha_{SPH} = \beta_{SPH} = 1 - 0{,}75x \\ \alpha_{FE} = \beta_{FE} = 0{,}75x \end{array}\right| \quad on \quad \Omega_g^0 \qquad [5]$$

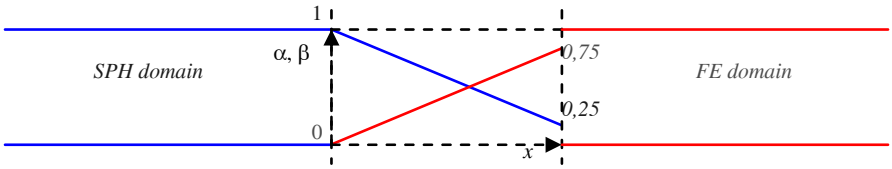

Figure 1. *Distribution of the weight paramater function*

NOTE. — The minimal value of the weight parameter functions in the SPH domain $\alpha = 0.25$ was selected in order to avoid the convergence to null mechanical characteristics on the boundary of SPH discretisation when the mesh is refined.

3.3. *Displacements and Lagrange multipliers interpolations*

The construction of the coupling matrices (based on Equation [4]) implies a volume integration. This integration is done numerically using the standard FEM Gauss integration scheme (co-ordinate $\underline{\xi}_q$, weight w_q). This implies the choice for the approximation functions of displacements and Lagrange multipliers in the domain Ω^0_g. The Lagrange multipliers are chosen to be interpolated with the FEM standard displacement's basis. It is also necessary to get the displacement values coming from SPH to the FEM Gauss points. These values $u^{\#}$ are obtained by a one-order "Moving Least Square" interpolation (Rabczuk *et al*., 2004):

$$\forall \underline{X}(x,y,z),\ \underline{u}^{\#}(\underline{X},t) = \sum_{i=1}^{N_{neighbour}} M_i(\underline{X})\underline{u}_i(t),$$
$$with \quad M_i(\underline{X}) = {}^{T}\underline{p}(\underline{X})\cdot \underline{\underline{A}}^{-1}(\underline{X})\cdot \underline{Q}\cdot w^0(\underline{X}-\underline{X}_i) \qquad [6]$$

where w^0 *is the SPH weighting function in total Lagrangian,*
M_i*, the generalised moving square interpolation function for SPH node i.*

3.4. *The coupling matrix*

The elementary coupling matrices between Lagrange multipliers and the two displacements discretisations are obtained by Gauss integration:

$$\underline{\underline{P}}^{FE}_{kj} = -\sum_{q=1}^{N_{PG}} N_k(\underline{\xi}_q)N_j(\underline{\xi}_q)w_q \quad and \quad \underline{\underline{P}}^{SPH}_{ki} = \sum_{q=1}^{N_{PG}} N_k(\underline{\xi}_q)M_i(\underline{\xi}_q)w_q \qquad [7]$$

with N_k*, the usual finite element shape function for FEM node k ,*
M_i*, the MLS interpolation function associated to SPH point i.*

The global matrix is (using the following order of unknowns $\underline{\lambda}$, $\underline{u}^{SPH}$ and $\underline{u}^{FE}$):

$$\underline{\underline{P}} = \frac{1}{2}\begin{bmatrix} 0 & 0 & -{}^{T}\underline{\underline{P}}^{FE} \\ 0 & 0 & {}^{T}\underline{\underline{P}}^{SPH} \\ -\underline{\underline{P}}^{FE} & \underline{\underline{P}}^{SPH} & 0 \end{bmatrix} \qquad [8]$$

3.5. *Explicit time integration*

The time integration is the central difference Newmark scheme. The state at the time step t^n is known. The algorithm is then:

– compute the external forces $\underline{F}^{n+1}{}_{ext}$ and internal $\underline{F}^{n+1}{}_{int}$ at the time step t^{n+1},

– compute the free accelerations $\underline{a}^{n+1}{}_{free}$, ignoring coupling forces:

$$\underline{a}^{n+1}_{free} = \underline{\underline{Mass}}^{-1}\left(\underline{F}^{n+1}_{ext} - \underline{F}^{n+1}_{\text{int}}\right) \qquad [9]$$

– compute the coupling forces ${}^{T}\underline{\underline{P}}\underline{\lambda}^{n+1}$ to impose the condition ${}^{T}\underline{\underline{P}}\underline{v}^{n+1} = 0$:

$$\underline{\lambda}^{n+1} = \left[\underline{\underline{B}}\right]^{-1} \cdot \underline{R}^{n+1} \quad with \quad \begin{array}{l} \underline{\underline{B}} = \underline{\underline{P}} \cdot \underline{\underline{\underline{\underline{Mass}}}}^{-1} \cdot {}^{T}\underline{\underline{P}} \\ \underline{R}^{n+1} = -2/\Delta t \, \underline{\underline{P}} \cdot \underline{v}^{n+1/2} - \underline{\underline{P}} \cdot \underline{a}_{free}^{n+1} \end{array} \qquad [10]$$

– compute the link accelerations induced by the coupling forces:

$$\underline{a}_{link}^{n+1} = \underline{\underline{\underline{\underline{Mass}}}}^{-1} \cdot {}^{T}\underline{\underline{P}} \cdot \underline{\lambda}^{n+1} \qquad [11]$$

– add link and free accelerations in order to obtain the real accelerations.

NOTE. — The matrices are considered constant in time and can be calculated and inversed only once. However this approximation is not valid if the volume's overlapping zone changes significantly: the matrices $\underline{\underline{B}}$ and $\underline{\underline{P}}$ have to be recomputed.

4. Numerical applications

This procedure, which follows the steps previously presented, has been introduced into the computer code EUROPLEXUS. This code will be used for all numerical applications shown in this paper.

4.1. *Description of the beam used for tests 1 to 3*

Several cases of loading were tested on a simple beam with the following characteristics:

– global length L = 36 mm, section S = 5×5 mm,

– elastic linear behavior (Young modulus E = 30 GPa, Poisson's ratio ν = 0),

– loads: initial velocity imposed, tensile test with displacements impose or bending test with forces impose.

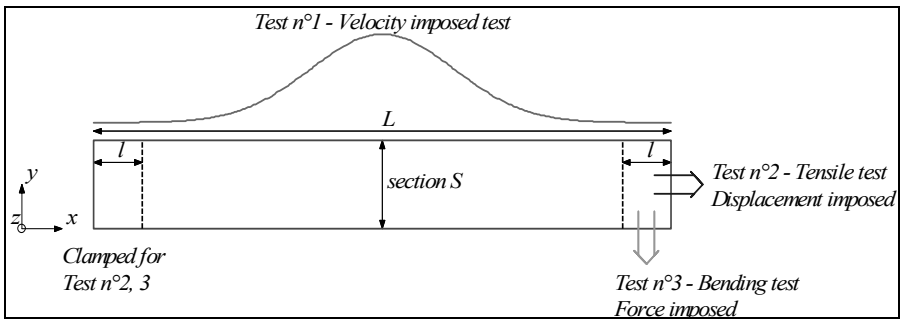

Figure 2. *Beam description. The 2 volumes of length l = 3 mm are the volumes where the boundary conditions are imposed*

The mesh grids used (Figure 4) are defined as:

– a purely FE mesh, constituted of 1mm-side cubes, called EF5,

– a mixed mesh, constituted of only one size of FE cubes identical to EF5 mesh and series of increasing fine SPH meshes. The mesh breaks up into SPH particles for $0 < x < 12$ mm and finite elements for $12 < x < 36$ mm.

Hence, each FEM cube of EF5 mesh is replaced by 1, 8, 27, 64, 125 SPH particles and the overlapping zone consists in 1 to 5 planes of SPH elements. These 5 mixed meshes will be called MXT 1:1, MXT 1:2, MXT 1:3, MXT 1:4, MXT 1:5.

4.2. *Results*

4.2.1. *Test n° 1*

In this first example, an initial velocity is imposed as it's proposed in the article (Rabczuk *et al*., 2004), such as:

$$v_x = e^{-0,025(x-x_m)^2} \qquad [12]$$

with x_m, co-ordinate median section.

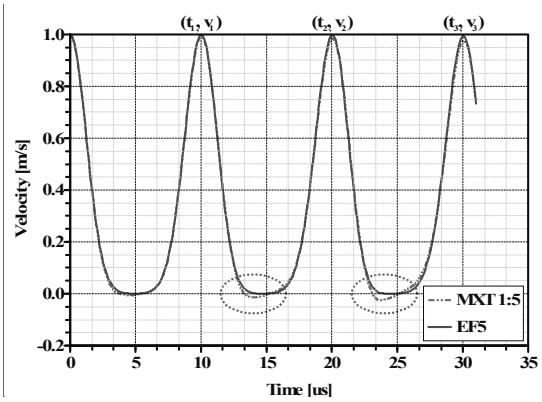

Figure 3. *Dynamic response: velocity of the beam's centre according to time*

Table 1. *Velocity of the beam's centre and travel time of waves*

	Time [μs]			***Centre velocity [m.s^{-1}]***		
	t_1	t_2	t_3	v_1	v_2	v_3
Analytical values	*9.97*	*19.94*	*29.91*	*1*	*1*	*1*
EF5	*10.03*	*20.06*	*30.02*	*0.999*	*0.997*	*0.995*
MXT1:5	*10.03*	*20.05*	*30.07*	*0.995*	*0.985*	*0.977*

4.2.2. *Test n° 2: tensile test with imposed displacement in direction x*

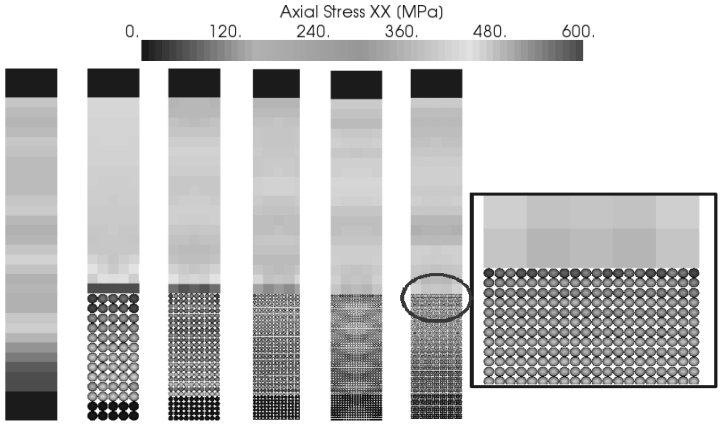

Figure 4. *Method convergence with refinement of SPH mesh. Axial stresses values* σ_{xx} *at* $t = 51\mu s$

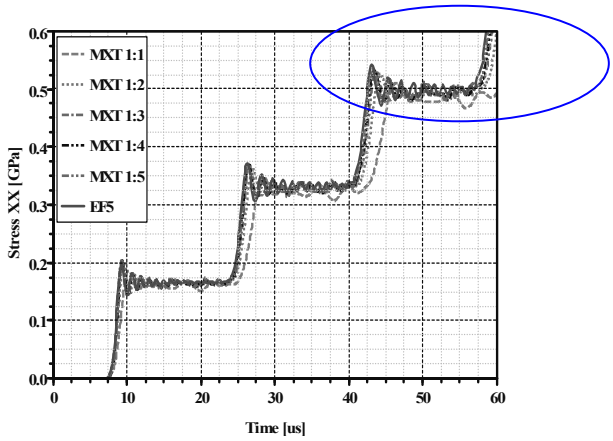

Figure 5. *Dynamic responses, EF5* vs. *(MXT1:1 to MXT1:5) meshes. Average axial stresses values at the clamping,* $\sigma_{xx} = f(t)$

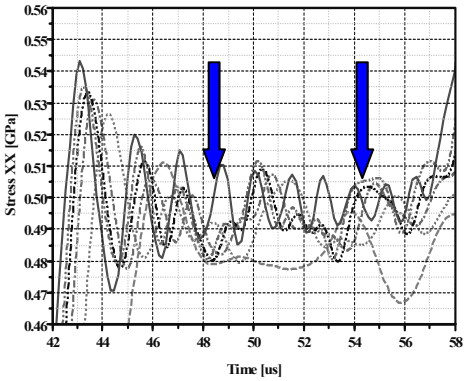

Figure 6. *Dynamic responses, EF5 vs. (MXT1:1 to MXT 1:5) meshes. Zoom into the blue circle of Figure 5*

4.2.3. *Test n°3: bending test with an imposed force in the direction y*

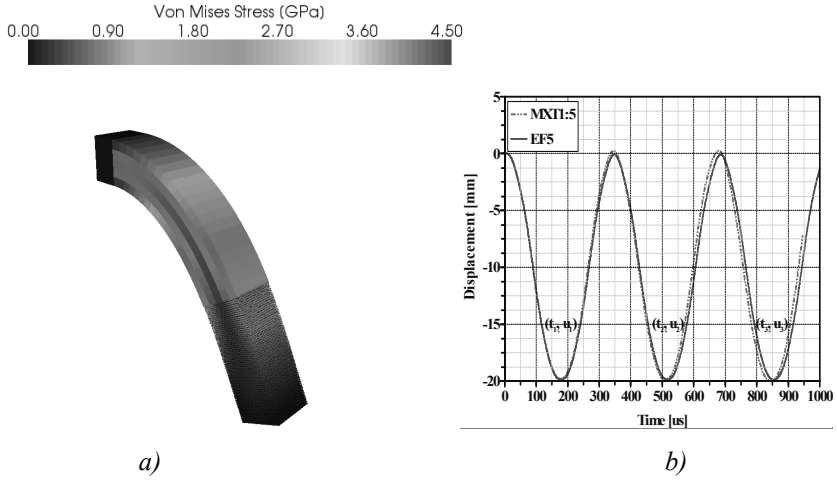

a) *b)*

Figure 7. *a) Von Mises stresses values at t = 860 μs, MXT1:5 mesh. b) Dynamic responses of EF5 vs. MXT1:5 meshes*

Table 2. *Maximal displacement and time corresponding, EF5 vs. MXT1:5 meshes*

	Time *[μs]*			***Amplitude*** *[mm]*		
	t_1	t_2	t_3	u_1	u_2	u_3
EF5	*178.2*	*516.9*	*854.9*	*19.91*	*19.89*	*19.91*
MXT1:5	*179.3*	*518.7*	*856.4*	*20.05*	*20.01*	*19.89*

4.2.4. *Conclusion*

The three tests show:

– the convergence of this hybrid method with the refinement of the mesh (Test n° 2 – Figures 4 and 6),

– a good global response in dynamics (Test n° 1 – Table 1; Test n° 3 – Table 2) of the hybrid beam.

However, the results highlight two consequences of the coupling used:

– a slight perturbation appears because of wave reflections on the interface (Test n° 1 – circles on the Figure 3; Test n° 2 – arrows on the figure 6),

– an overstress concentrated on the interface which decreases with the refinement of SPH mesh (Test n° 2 – Figure 4)

4.3. Model of projectile's impacts on concrete slabs

4.3.1. *Behavior law of concrete under impact*

The behavior law is based on the work of (Mazars, 1984), extended in this paper to dynamics. Indeed, under a compression load, the equivalent deformation is given from the positive deformations. However, under fast loads, ruptures in compression are observed without being predicted with this choice of equivalent deformation. So, the measure of the equivalent deformation was modified in order to predict damage of material under a fast compression load, such as:

$$\tilde{\varepsilon} = \sqrt{\sum_i \left(\mathrm{H}_i \varepsilon_i\right)^2} + \sqrt{2}\nu \sqrt{\sum_i \left(\left(1 - \mathrm{H}_i\right)\varepsilon_i\right)^2} \qquad [13]$$

with H_i*, Heaviside function.*

Two other modifications, because of the use in dynamics, have been added to the behavior law:

– a dependence to the strain velocity, noted by many authors with experimental tests on rocks or concrete, (Blanton *et al.,* 1981),

– a limitation of the growth rate damage in order to avoid the artificial localisation and the dependence with the mesh refinement. (Suffis *et al.,* 2002).

The model uses 7 parameters: the threshold of initial damage ε_{D0}, a couple (A_t, B_t) defining the behavior law in traction, and a couple (A_c, B_c) for the law in compression, one more parameter for the delay effect and a last one for the dependence to the strain rate.

4.3.2. *Description of simulations and experiments*

Zhang *et al.,* (2005) realised lots of experiments in order to characterise the resistance of the high performance concrete under impact. We choose two tests to simulate: 2 impacts of a 15g projectile with 12.6 mm-diameter ogival head on a 300×170×150 mm concrete slab. The characteristics of impacts are:

– impact velocities: 678 and 650 $m.s^{-1}$,

– ultimate strength: traction – 30.3 MPa; compression - 187 MPa,

– Young modulus: 30 GPa; Poisson's ratio: 0.22; density: 2 300 $kg.m^{-3}$.

The numerical model is composed of 3 288 finite elements and 252 000 SPH. A support condition is imposed on all lower surface and a PINBALL algorithm is used for the management of the contact "impactor – target". (Belytschko, 1991)

4.3.3. Results

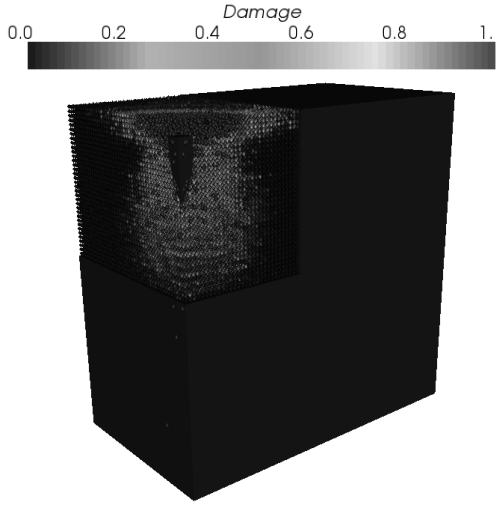

Figure 8. *Deformed and final damage of simulation*

Table 3. *Experiment vs. simulation*

	Velocity[m.s^{-1}]	***Depth [mm]***	***Crater diameter [mm]***
Experiments	*678*	*33*	*70*
	650	*28*	*57*
Average	***664***	***30,75***	***63,5***
Simulation	***664***	***30,25***	***60,5***

The results show a good quality of the predicted penetration depth and the dimension of the crater on this complex example.

5. Conclusion

We presented the general formalism which has been implemented in EUROPLEXUS computer code. The validation was made on simple benchmark for a coupling with an overlapping domain between SPH particles and finite elements and compatible mesh. The method proposed seems to well couple a FE mesh and SPH particles in the linear elastic problems. Then, the comparison between experiments and simulations of impact shows that the method can be used for complex nonlinear problems.

6. References

Belytschko T., "Contact-Impact by the Pinball Algorithm with Penalty and Lagrangian Methods", *Int. J. Num. Meth. Engrg.*, 1991, vol. 31, p. 547-572.

BenDhia H., « Problèmes mécaniques multi-échelles : la méthode arlequin », *C. R. de l'Académie des Sciences*, Série IIb, 1998, vol. 36, p. 899-904.

Blanton T.L., "Effect of strain rates from 10^{-2} to 10 s^{-1} in triaxial compression tests on three rocks", *Int. J. Rock Mech. Min. Sci.*, 1981, vol. 18, p. 47-62.

Farhat C., Chen P., Mandel J., "A stable Lagrange multiplier based domain-decomposition method for time-dependent problems", *Int. J. Num. Meth. Engrg.*, 1995, vol. 50, p. 199-225.

Gravouil A., Combescure A., "Multi-time-step explicit-implicit method for non-linear structural dynamics", *Int. J. Num. Meth. Engrg.*, 2001, vol. 50, p. 199-225.

Mazars J., Application de la mécanique de l'endommagement au comportement non linéaire et à la rupture du béton de structure, Thèse de doctorat d'état, Université Paris VI, 1984.

Rabczuk T., Belytschko T., Xiao S.P., "Stable particle methods on Lagrangian kernels", *Comp. Meth. Appl. Engrg.*, 2004, vol. 193, p. 1035-1063.

Rabczuk T., Xiao S.P., Sauer M., "Coupling of mesh-free methods with finite elements: basic concepts and test results", *Commun. Num. Meth. Engrg.*, 2006, vol. 22, p. 1031-1065.

Rateau G., Méthode Arlequin pour les problèmes mécaniques multi-échelles. Application à des problèmes de jonction et de fissuration de structures élancées, Thèse Ecole Centrale Paris, 2003.

Suffis A., Combescure A., « Modèle d'endommagement à effet retard, analyse numérique et analytique de l'évolution de la longueur caractéristique », *Revue Européenne des Eléments Finis*, vol. 11, 2002, p. 593-620.

Zhang M.H., Shim V.P.W., Lu G., Chew C.W., "Resistance of high-strength concrete to projectile impact", *Int. Journal of Impact Engineering*, vol. 31, n° 7, 2005, p. 825-841.